

Hydrogen Production by water Electrolysis with an Ultrathin Anion-exchange membrane (AEM)

Immanuel Vincent, Andries Kruger and Dmitri Bessarabov*

DST HySA Infrastructure Centre of Competence, Faculty of Engineering,
North-West University, Potchefstroom, 2520, South Africa

*E-mail: Dmitri.bessarabov@nwu.ac.za

Received: 30 August 2018 / Accepted: 5 October 2018 / Published: 5 November 2018

A new ultrathin anion exchange membrane (AEM) is proposed for low cost AEM electrolysis. The advantages that thin membranes offer include reduced mass transport resistance and ohmic resistance. A membrane electrode assembly (MEA) with a thinner membrane will have improved hydroxide ion transfer due to the shorter ion transfer pathway. We fabricated a MEA with a commercially available ultrathin A-901 membrane (9 μm thick) and non-noble metal catalysts. We determined the efficiency and stability of this ultrathin membrane using electrochemical impedance spectroscopy. The best performance recorded was 400 mA cm^{-2} at 1.94 V at 50 $^{\circ}\text{C}$. Over a period of 200 h, the voltage increase was only $200 \mu\text{V h}^{-1}$, which is <60% that of the more commonly used A-201 membrane. The ultrathin A-901 membrane exhibited slightly higher performance compared to the A-201 for a given catalyst, catalyst loading, and electrolyte concentration. Acta 3030[®] (CuCoO_x) and Acta 4030[®] ($\text{Ni}/(\text{CeO}_2\text{-La}_2\text{O}_3)/\text{C}$) were employed as the oxygen evolution reaction and hydrogen evolution reaction catalysts, respectively.

Keywords: A-901 AEM membranes, A-201 AEM membranes, Membrane electrode assembly, Oxygen evolution reaction, Hydrogen evolution reaction, Electrochemical impedance spectroscopy.

1. INTRODUCTION

The hydrogen energy concept as an energy carrier can provide a carbon-neutral option for the storage and distribution of energy [1–4]. Currently, hydrogen is produced from fossil fuels such as coal, crude oil, natural gas, etc., by steam reforming, thermal cracking, and coal gasification [5]. It can also be produced from renewable sources such as solar, wind, water, etc., by biomass conversion, thermochemical processes, photolysis, and electrolysis [6]. Hydrogen production from water electrolysis is one of the technologies that is attracting increasing attention because of the hydrogen purity and niche applications, such as power-to-gas production. The two main types of electrolysis are

proton exchange membrane (PEM) electrolysis and alkaline membrane electrolysis [7]. The electricity required to produce hydrogen via electrolysis can be supplied from renewable sources, such as solar [8].

In PEM electrolysis, a PEM (e.g., Nafion) is used as a solid polymer electrolyte [9]. The PEM electrolyser can operate at a current density of 2000 mA cm^{-2} at about 2.1 V at $90 \text{ }^\circ\text{C}$ [9]. However, due to the highly acidic environment, this technology is limited to using platinum group metals as electrocatalysts [10]. Alkaline electrolysis can be operated with less expensive non-platinum group metal catalysts and a separator, such as a diaphragm [8]. However, the 30% KOH electrolyte is highly corrosive and leads to the formation of K_2CO_3 when in contact with the ambient air, which subsequently reduces the efficiency of the electrolyser [11].

To reduce the cost of electrolysis and increase the efficiency, a non-platinum group metal catalyst and less expensive membrane system is essential. Recently, polymer-based anion exchange membrane (AEM) electrolysis was introduced and non-platinum catalysts were used [12]. AEM electrolysis is a combination of a PEM and alkaline electrolysis technology [13]. The concept of AEM electrolysis with MEA is illustrated in Fig. 1.

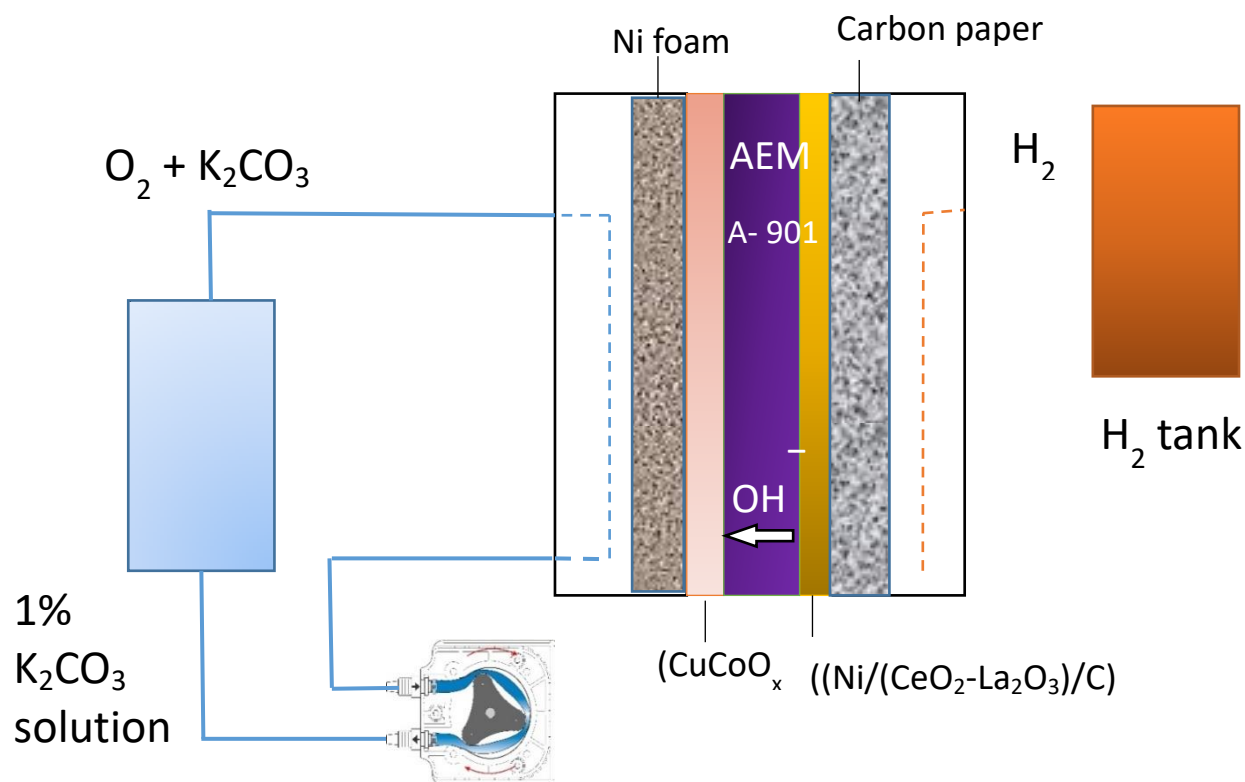
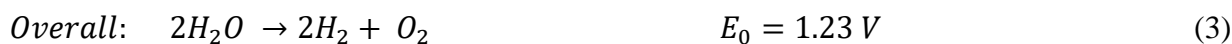


Figure 1. Schematic of the anion exchange membrane (AEM) electrolysis with MEA.

An AEM electrolysis system generally consists of an alkaline AEM and non-noble metal electrocatalysts for both the anode and the cathode. Dilute 1% K_2CO_3 is used as electrolyte to provide the ionic conductivity. An optimum current density of 500 mA cm^{-2} is achieved at 1.9 V [13].

The AEM is one of the key components that determines the performance of an AEM electrolyser. The function of the AEM is to transport hydroxyl ions (OH^-) from the cathode to the

anode, and to act as a barrier for electrons and gases that are produced by the electrochemical reaction [13].



The AEM is typically composed of a polysulfone (PSF) or polystyrene cross-linked with divinylbenzene. The conduction of OH^- arises from the presence of ion exchange groups such as $-\text{NH}_3^+$, $-\text{RNH}_2^+$, $-\text{RN}^+$, $-\text{R}_2\text{N}^+$, $-\text{R}_3\text{P}^+$, $-\text{R}_2\text{S}^+$, or quaternary ammonium salts [13] in the polymeric structure. The desirable properties of an efficient AEM are listed in [12 -15, 22], these include high mechanical, thermal and chemical stability; high ionic conductivity; and low gas permeability.

One of the commercially available polymer electrolytes that is used in AEM electrolysis is the A-201 membrane (Tokuyama Corp., Japan). The backbone of A-201 is a linear hydrocarbon and the functional groups are quaternary ammonium groups [16].

Alternative polymer backbones and functional groups for AEMs have also been developed and evaluated for AEM electrolysis [17,18].

The membrane electrode assembly (MEA) for AEM water electrolysis includes the AEM, ionomer, and anode and cathode catalyst layers. The MEA can be fabricated by various methods [19 - 21].

The internal resistance of the membrane is a function of membrane thickness, which directly affects the cell overpotential. The thickness of the AEM used, commercially, in AEM electrolysis is 40–80 μm [22]. The most commonly used AEM is the commercially available A-201 (membrane thickness 28 μm ; Tokuyama Corp.) [21]. Although thinner membranes exhibit better performance, it is known that they are not mechanically stable. When ultrathin membranes are used, the following benefits can be achieved. The mass transport resistance of water penetration is reduced. The transport resistance of ultrathin thickness membrane facilitates the transport of reactant and product. However, one of the main disadvantages of using ultrathin membranes is that the membranes becomes physically damaged; holes are formed in membranes when the electrolyser cell is subjected to tightening [22]. The gas cross-over in such membranes also needs to be studied.

In this study, we used the commercially available ultrathin A-901 membrane (Tokuyama Corp.) for the AEM electrolysis. This ultrathin membrane has a thickness of only 9 μm . To the best of our knowledge, it has not yet been considered as a candidate membrane for AEM water electrolysis. The reduced membrane thickness should result in an increased rate of OH^- transfer due to the shorter electron and ion transfer pathway [23]. Furthermore, during the electrolysis process, a strong electric field is created at the interface of the electrocatalyst and membrane, hence the OH^- generated by the HER migrates under a strong electric field [23]. It is expected that the reduced membrane thickness will lead to an increase in MEA performance. It is also important to note that the chemical structure of the A-901 is not disclosed in the public domain.

We fabricated our MEA with the ultrathin A-901 membrane and PFM-free metal catalyst. We determined the efficiency and stability of the membrane using electrochemical impedance spectroscopy (EIS). Using EIS, the different resistances that contribute to the total cell voltage can be

separated (kinetic resistance from the diffusional impedance). We now report on the efficiency and stability of this new ultra-thin membrane.

2. EXPERIMENTAL

2.1. Preparation of the MEA

The MEAs were prepared based on a previously published CCS method [22]. Acta 3030[®] (CuCoO_x) and Acta 4030[®] (Ni/(CeO₂-La₂O₃)/C) were employed as the oxygen evolution reaction (OER) and hydrogen evolution reaction (HER) catalysts, respectively. The anode catalyst layer was prepared from a homogenous ink comprising Acta 3030, deionized water (DI), isopropyl alcohol (IPA), and alkaline ionomer (ionomer I₂; Acta Spa, Italy) solution. The cathode catalyst ink was a mixture of Acta 4030, IPA, Teflon AF amorphous fluoroplastic solution (DuPont, USA), and DI. The loadings of the OER and HER catalysts were ~30 and ~7.4 mg cm⁻², respectively. As mentioned earlier, the ultrathin AEM used in the electrolyser was the A-901 (membrane thickness 9 μm; Tokuyama Corp.). The membrane was sandwiched between the anode and cathode GDEs to form the MEA.

2.2. AEM electrolysis set-up

The electrolyser cell used in this study had an active area of 5 cm², similar as described in [22]. The flow field plates were compressed between two aluminium end plates. Preheated 1% K₂CO₃ solution was used as electrolyte. The electrolyte was circulated through the anode side with a peristaltic pump. In this AEM electrolysis set-up, the electrolyte was fed only to the anode side to allow higher discharge pressure of hydrogen at the cathode side. DC power supply (TDK-Lambda) was used. The temperature was maintained at 60 °C, using a water bath (F12; Julabo, Germany). The system was controlled by Labview[®] software.

2.3. Electrochemical characterisation of AEM electrolysis cell by EIS

Electrochemical impedance spectroscopy was performed using a Gamry 600 potentiostat. The perturbation current used was in the range 0.5–2.5 A. The impedance was measured with an AC current signal in the frequency range 50–100 kHz, superimposed on the DC polarisation current. The amplitude of the AC signal was less than 10% of the applied DC current.

An equivalent circuit model was developed and fitted using the Gamry software. See Fig. 2. Details of the equivalent circuit are the following: I_{stray} (Ω. cm²), resistances of the electrical wires for both anode and cathode; HFR (Ω. cm²), membrane resistance; R_{f cathode} (Ω. cm²), cathodic polarisation resistance of the HER; R_{f anode} (Ω. cm²), anodic polarisation resistance of the OER; Y_{o cathode} and Y_{o anode} (F.cm⁻².sⁿ⁻¹), frequency independent constants of the electrolyte interface.

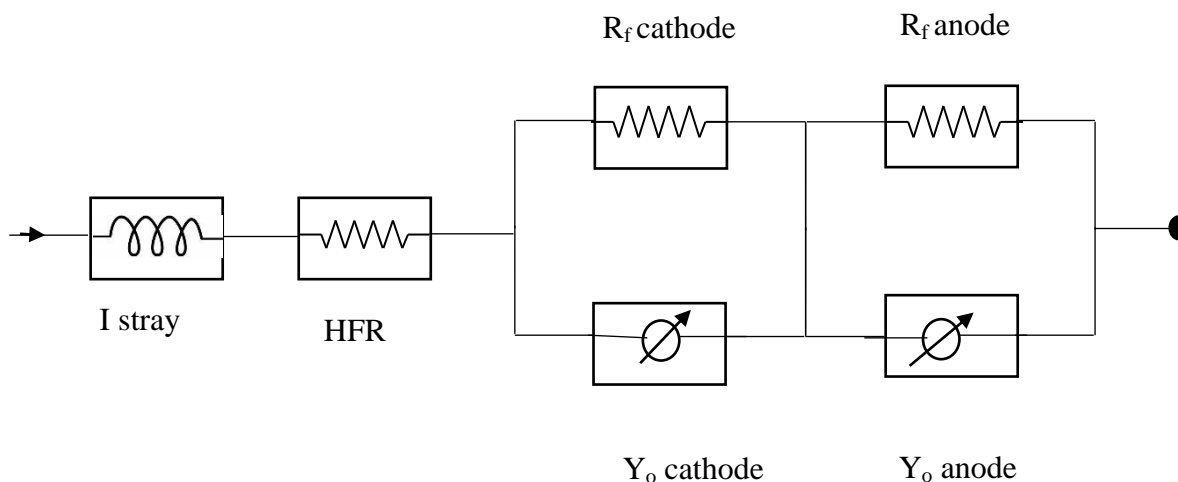


Figure 2. Equivalent circuit model for the EIS analysis.

3. RESULTS AND DISCUSSION

3.1 Performance of the MEA

The performance of the MEA with the ultrathin membrane was evaluated at 50 °C. See Fig. 3. Prior to recording any measurements, the electrodes were activated for 2 h, by maintaining a current density of 1000 mA cm⁻². Polarisation curves were recorded in the range 0–1000 mA cm⁻², in 50 mA cm⁻² steps. Three regions were identified: the activation polarisation region, ohmic polarisation region, and mass transport polarisation region. The activation polarisation region was found at low current density, the mass transport region at higher current density, and the ohmic resistance region was found in all the regions. The latter is however dominant at higher current density. With an increase in electrolysis current density, the mass transport becomes prominent [24]. The cell voltage sharply increased up to a current density of 200 mA cm⁻². At higher current density the voltage increase was insignificant.

The MEA performance exhibited by the ultrathin A-901 AEM was compared with that of the more commonly used/conventional Tokuyama A-201 AEM. The former showed slightly higher performance than the latter. At current density 50–300 mA cm⁻², the performance was significantly higher; however, at higher current density, the difference between the two was insignificant. The better performance achieved with the A-901 membrane probably originates from its higher ion conductance (A-201: 11 vs. A-901: 29 mS cm⁻²) and faster water transport within the membrane. As the current density increases, the resistance of the cells, with the A-201 and with the A-901 membrane, increases. This is indicative of mass transport issues, such as electroosmotic drag of water, induced by OH⁻ migration toward the anode. The ionic conductivity of A-201 is slightly higher than that of A-901. The ion exchange capacity of both membranes is 1.8 mmol g⁻¹. The cell performance was stable for both A-201 and A-901, probably due to sufficient water transport to the cathode. Performance of A-901 and a-201 at 500 mA cm⁻² at 50° C is shown in Figure 4.

The performance achieved with the ultrathin A-901 was comparable to that achieved with the conventional A-201, as reported by Pavel et al. [13] and Leng et al. [21]. In our study, at 50 °C, a current density of 400 mA cm⁻² was achieved at cell potential 1.94 V. At 50 °C, Leng et al. and Pavel et al. achieved 400 mA cm⁻² at cell potentials 1.82 and 1.80 V. Although the observed increase in performance of the A-901 could be due to a difference in membrane thickness, the chemical composition of the polymers may also be a factor. However, in this study, we were unable to consider chemical differences between the A-901 and A-201 as the composition of the A-901 is proprietary/unavailable. Furthermore, in our study, we obtained a relatively high voltage, 0.12 V higher than that reported by Leng et al [21]. They used a high loading of conventional noble metal electrocatalyst. The cell voltage of our electrolyser was, however, slightly higher than that reported by Pavel et al [13].

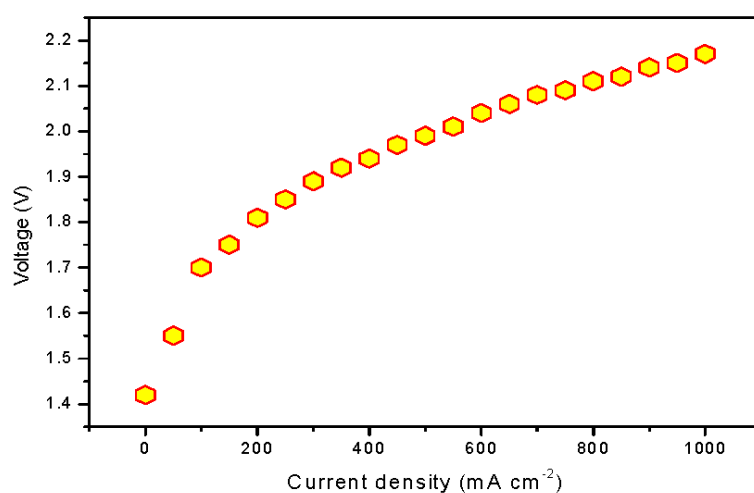


Figure 3. Polarization curve recorded for AEM electrolysis at 50 °C. (Catalyst loading of anode ~30 mg cm⁻² and cathode ~7.4 mg cm⁻²; A-901 used as AEM).

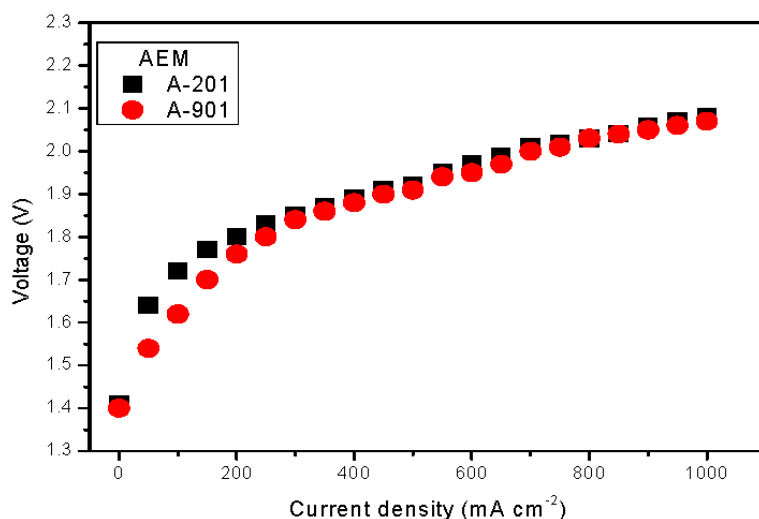


Figure 4. Performance of A-901 and A-201 at 500 mA cm⁻² at 50 °C. (Catalyst loading of anode ~30 mg cm⁻² and cathode 7.4 mg cm⁻².)

Fig. 5 shows the relationship between the current and voltage at various temperatures (in the range 40–80 °C). A current density of 1000 mA cm^{-2} was achieved at voltages 2.21, 2.17, 2.14, and 2.09 V at 40, 50, 60, and 80 °C respectively. At 40 °C, 500 mA cm^{-2} was achieved at 2.03 V. The voltage decreased when the temperature was increased similar as described in [22]. The increase in temperature results in increase in the ionic conductivity of the AEM and the electrocatalytic activity, while mass transport resistance was reduced [13,25].

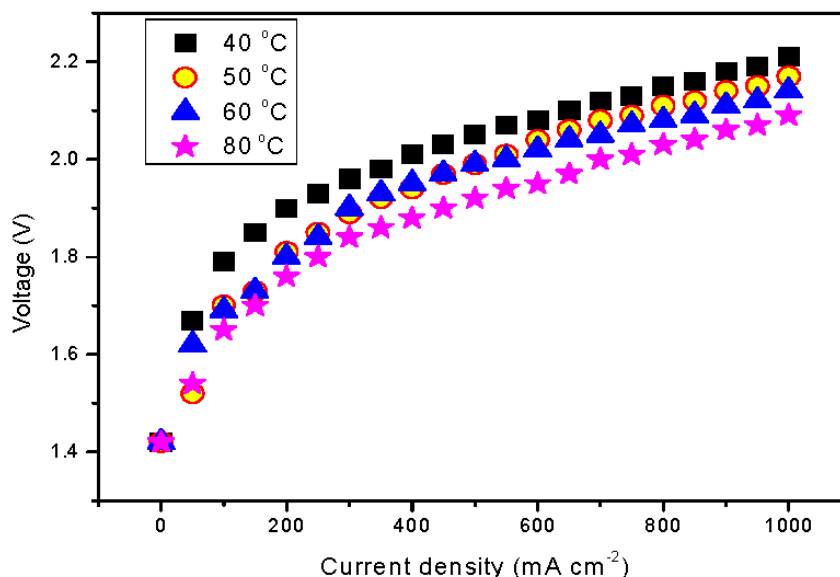


Figure 5. Polarisation curves at different temperatures. (Catalyst loading of anode $\sim 30 \text{ mg cm}^{-2}$ and cathode $\sim 7.4 \text{ mg cm}^{-2}$; A-201 used as AEM).

3.2 Stability of the MEA

The stability of an AEM in water electrolysis mode is an important factor. AEMs are prone to chemical degradation due to nucleophilic attack on the cationic fixed charge sites by the OH^- . Nucleophilic attack causes a decrease in the number of anion exchange groups, which reduces the OH^- conductivity.

AEM stability was evaluated at 500 mA cm^{-2} and $50 \text{ }^\circ\text{C}$ over a period of 200 h. The ultrathin A-901 exhibited a stable performance over this period. See Fig. 6. The voltage increased from 2.13 to 2.17 (rate of voltage increase $200 \text{ } \mu\text{V h}^{-1}$). In a previous study of ours [22], the A-901 was compared with the A-201. Experiments were carried out at 500 mA cm^{-2} and $60 \text{ }^\circ\text{C}$. The voltage increased from 1.98 to 2.08 (rate of voltage increase $500 \text{ } \mu\text{V h}^{-1}$). The rate of voltage increase exhibited by the A-901 was lower than recorded for the A-201. The rate of voltage increase was determined from the voltage difference between 0 and 200 h, and the voltage difference was divided by the total number of hours. The improved stability was mainly attributed to the water uptake of the A-201, which was 25%, whereas that of the A-901 was only 15%. The higher water uptake may reduce the cell potential, which will reduce the stability of the membrane [26]. Furthermore, the more intimate contact between

membrane and catalyst layer reduces the chances of disassociation of catalyst particles and the ionomer during stability testing, leading to improved long-term performance.

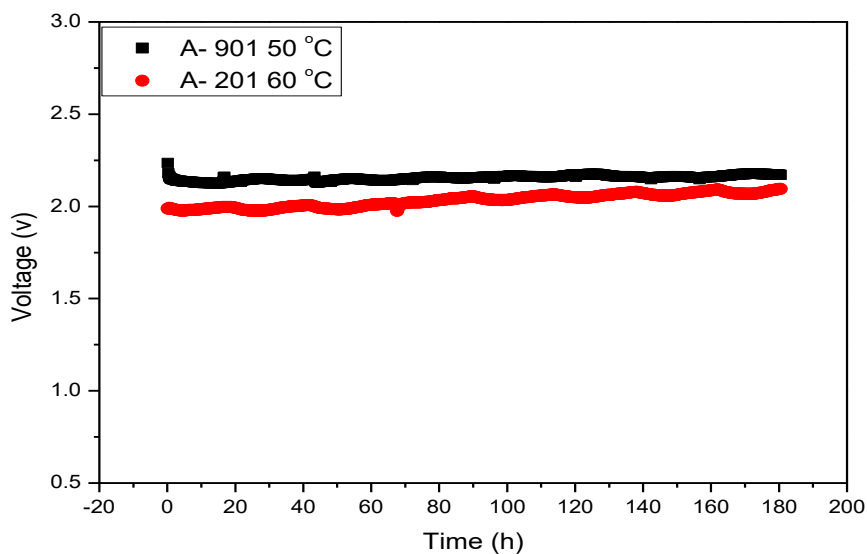


Figure 6. Stability of the MEA over 200 h: A-901 (at 50 °C) and A-201 (at 60 °C), at 500 mA cm⁻² and. (Catalyst loading of anode ~30 mg cm⁻² and cathode 7.4 mg cm⁻².)

3.3 MEA characterisation by EIS

Electrochemical impedance spectroscopy is an interesting and useful tool for characterising the MEA of an AEM electrolyser. It enables the determination of the major resistances, such as electrical resistance, ohmic resistance, and electrochemical reaction resistance. The ohmic resistance depends on the electrolyte concentration, the membrane, and the distance between membrane and electrodes [27]. The gas bubbles produced from the electrochemical reaction at the electrode surfaces cause mass transport resistance [24]. We measured the overall resistance under in situ conditions of a running AEM water electrolyser. The current and temperature were varied. The gas production of H₂ and O₂ takes place at the back side of the GDLs, hence the mass transport limitation can be considered to be zero.

The Nyquist plot (a parametric *plot* of a frequency response, commonly used to assess the stability of a system) is commonly depicted as a semicircle. It involves a semicircle loop at high frequency and a straight line at low frequency. The semicircle loop at high frequency is attributed to the charge transfer resistance and the slope at low frequency is related to the diffusion. Fig. 7 shows a typical Nyquist plot obtained for the A-901, together with a fitting obtained by the model described (see Experimental).

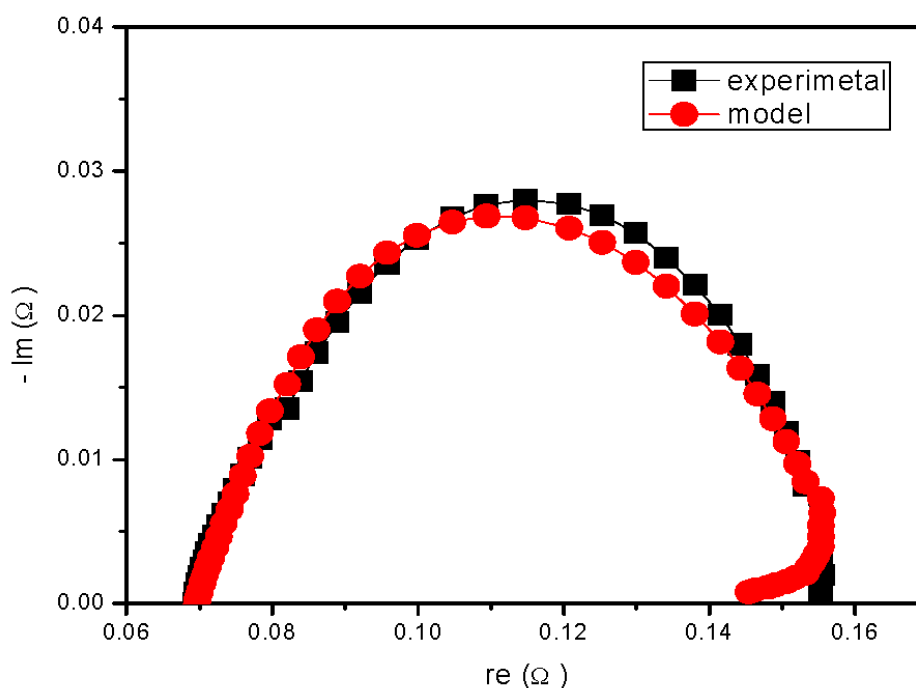


Figure 7. Nyquist plot obtained for A-901 and mathematical model fitted to experimental data to obtain resistance values. (Catalyst loading of anode $\sim 30 \text{ mg cm}^{-2}$ and cathode $\sim 7.4 \text{ mg cm}^{-2}$).

To determine the effect of current density, the impedance was measured at $50 \text{ }^\circ\text{C}$ in the current range $0.5\text{--}2.5 \text{ A}$. To determine the effect of temperature, the impedance was measured at 2 A at various temperatures: $40, 50, 60,$ and $80 \text{ }^\circ\text{C}$.

Fig. 8 shows the real and imaginary impedance data obtained as a function of current density for A-901 at $50 \text{ }^\circ\text{C}$. The semicircle shape of the impedance spectra indicates that there is little to no mass transfer at lower current density; the polarisation resistance becomes insignificant, and only ohmic resistance (electronic and ionic resistance) exists. The single semicircle of the impedance spectra is an indication of capacitive behaviour. It also reveals that two-electron transfer occurs simultaneously (the HER at the cathode and the OER at the anode) [28]. The half-cell measurement from the model reveals that the contribution of the OER to the overall impedance is high. This is due to greater thickness of the anode catalyst layer. Increase in the thickness of the catalyst layer results in an increase in the mass transport and the electronic resistance. The OER kinetics are slow and strongly irreversible at ambient temperature [27]. The overall impedance confirms that the OER is the rate-determining step. At low frequencies (close to stationary conditions), the polarisation resistance of the cathode is much lower (~ 8 times) than the polarisation resistance of the anode.

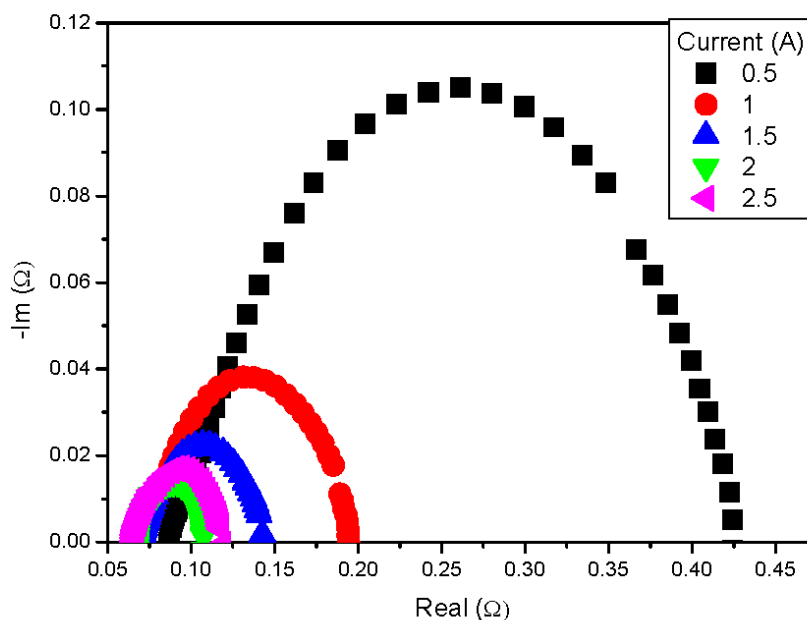


Figure 8. Nyquist plot of A-901 measured as a function of current. (Catalyst loading of anode $\sim 30 \text{ mg cm}^{-2}$ and cathode $\sim 7.4 \text{ mg cm}^{-2}$; A-901 used as AEM).

Fig. 9 shows the impedance data obtained as a function of cell temperature for A-901. The current density varied between 0.5 and 2.5 A, with steps of 0.5 A. Membrane resistance decreased with increasing current; resistance was 87 m Ω and 72 m Ω for 0.5 and 1 A, respectively. The cathodic resistance (R_{ct}) decreased from 169 to 101 m Ω (reduction decreased by 40%) for 0.5 and 1 A. The OER R_{ct} decreased from 2.6 to 0.62 m Ω for 0.5 and 1 A, respectively. In all cases, the resistances were high for 0.5 A, while resistances for the other currents were significantly reduced.

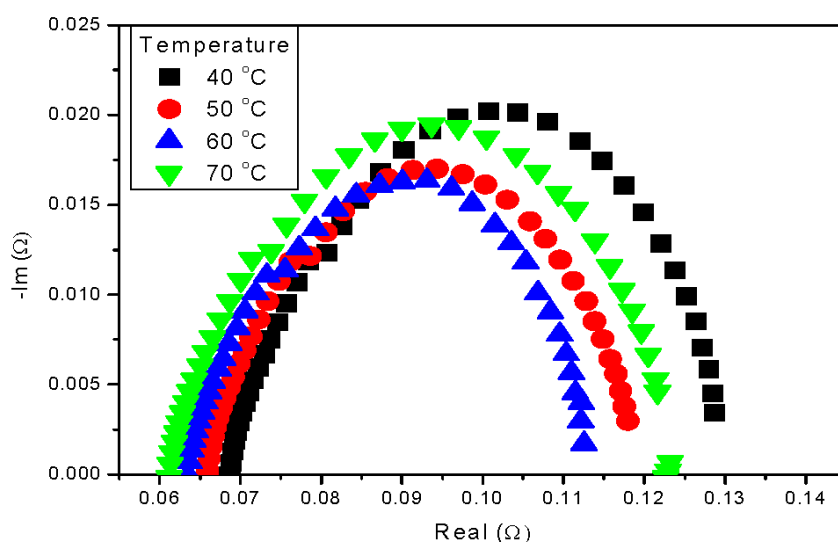


Figure 9. Nyquist plot for A-901 as a function of cell temperature. (Catalyst loading of anode $\sim 30 \text{ mg cm}^{-2}$ and cathode $\sim 7.4 \text{ mg cm}^{-2}$; A-901 used as AEM).

Table 1 shows the results obtained for the A-901, as a function of temperature, by the mathematical modelling. The data presented was obtained at 1 A. The contribution of the HFR (membrane resistance) to the overall resistance was too low. The HFR was in the range of 60–70 m Ω . However, the membrane resistance by the A-901 decreased with increasing temperature and with increasing current.

At cell voltages higher than approximately 1.8–1.9 V, cell losses due to charge transfer processes become negligible and the impedance of the AEM cell was mostly ohmic. There was no significant change in the HFR over the temperature range 40–70 °C; the reduction was only 69–63 m Ω . The R_{ct} was significantly reduced, from 3.92, 1.72, 0.7, and 0.56 m Ω . However, at this point, no clear explanation can be given for the reduction of the double-layer capacitance.

Table 1. Various resistances obtained for A-901, as a function of temperature, by the mathematical modelling

	40 °C	50 °C	60 °C	80 °C
HFR ($\Omega \cdot \text{cm}^2$)	72	70	67	65
R_f cathode ($\Omega \cdot \text{cm}^2$)	123	70	37	51
Y_f cathode ($\text{F} \cdot \text{cm}^{-2} \cdot \text{s}^{n-1}$)	192.3	155	153	101
Y_o anode ($\text{F} \cdot \text{cm}^{-2} \cdot \text{s}^{n-1}$)	692	717	788	721
R_f anode ($\Omega \cdot \text{cm}^2$)	8.41	7.5	7.025	5.392

4. CONCLUSIONS

The ultrathin membrane A-901, which has a thickness of only 9 μm , was evaluated as a candidate membrane for AEM water electrolysis. We investigated the efficiency and stability of this membrane. The best performance achieved was 400 mA cm^{-2} at 50 °C at cell potential 1.94 V. The ultrathin A-901 membrane exhibited slightly higher performance than that of the conventional A-201 membrane. The voltage increase was only 200 $\mu\text{V h}^{-1}$, which is less than 60% of that obtained for the conventional A-201. The improved stability of the A-901 is mainly due to its higher water uptake. EIS analysis revealed that the contribution of the OER to the overall cell resistance is high. This is mainly due to the greater catalyst thickness of the anode catalyst layer. Reduction of the anode catalyst layer is essential to improve AEM electrolyser performance. Investigations into membrane stability revealed that degradation of the MEAs with A-901 was lower than with A-201, indicating that the ultrathin membrane A-901 membrane is a suitable candidate membrane for reducing the operational costs of electrolysis.

References

1. G. W. Crabtree and M. S. Dresselhaus, *MRS Bull.*, 33 (2008) 421.
2. J. Tollefson, *Nature* 464 (2010) 1262.
3. European Commission, Brussels. Hydrogen Energy and Fuel Cells, 2003.
4. A. Midilli and I. Dincer, *Int. J. Hydrogen Energy*, 33 (2008) 4209.
5. S. Ahmed and M. Krumpelt, *Int. J. Hydrogen Energy*, 26 (2001) 291.
6. J. D. Holladay, J. Hu, D. L. King and Y. Wang, *Catal. Today*, 139 (2009) 244.
7. P. Millet and S. Grigoriev, Water electrolysis technologies, Renew. Hydrog. Technol. Prod. Purification Storage, Appl. Saf., 2013, 19.
8. A. Manabe, M. Kashiwase, T. Hashimoto, T. Hayashida, A. Kato, K. Hirao, I. Shimomura and I. Nagashima, *Electrochim. Acta*, 100 (2013) 249.
9. M. Carmo, D. L. Fritz, J. Mergel and D. Stolten. *Int. J. Hydrogen Energy*, 38 (2013) 4901.
10. P. Millet, N. Mbemba, S. A. Grigoriev, V. N. Fateev, A. Aukauloo and C. Etiévant. *Int. J. Hydrogen Energy*, 36 (2011) 4134.
11. K. Zeng and D. Zang, *Prog. Energy Combust. Sci.*, 36 (2010) 307.
12. I. Vincent and D. Bessarabov. *Renew. Sustain. Energy Rev.*, 81 (2018) 1690.
13. C. C. Pavel, F. Cecconi, C. Emiliani, S. Santiccioli, A. Scaffidi, S. Catanorchi and M. Comotti, *Angew. Chem. Int. Ed. Engl.* 5,3 (2014) 1378.
14. G. Merle, M. Wessling and K. Nijmeijer, *J. Membr. Sci.*, 377 (2011) 1.
15. S. Lu, J. Pan, A. Huang, L. Zhuang and J. Lu, *Proc. Natl. Acad. Sci.*, 105 (2008) 20611.
16. K. Fukuta, Tokuyama Corporation, 2011. AMFC Workshop 2011: Electrolyte Materials for AMFCs and AMFC Performance.
17. M. Faraj, M. Boccia, H. Miller, F. Martini, S. Borsacchi, M. Geppi and A. Pucci, *Int. J. Hydrogen Energy*, 37 (2012) 14992.
18. Y.-C. Cao, X. Wu and K. Scott, *Int. J. Hydrogen Energy*, 37 (2012) 9524.
19. H. Tang, S. Wang, S. P. Jiang and M. Pan, *J. Power Sources*, 170 (2007) 140.
20. S. Song, H. Zhang, X. Ma, Z. Shao, R. T. Baker and B. Yi, *Int. J. Hydrogen Energy*, 33 (2008) 4955.
21. Y. Leng, G. Chen, A. J. Mendoza, T. B. Tighe, M. A. Hickner and C.-Y. Wang, *J. Am. Chem. Soc.*, 134 (2012) 9054.
22. I. Vincent, A. Kruger and D. Bessarabov, *Int. J. Hydrogen Energy*, 42 (2017) 10752.
23. M. Mamlouk, P. Ocon and K. Scott, *J. Power Sources*, 245 (2014) 915.
24. D. Zhang and K. Zeng, *Ind. Eng. Chem. Res.*, 51 (2012) 13825.
25. D. R. Dekel, S. Willdorf, U. Ash, M. Amar, S. Pusara, S. Dhara, S. Srebnik and C. Diesendruck, *J. Power Sources*, 375 (2018) 351.
26. Q. Duan, S. Ge and C. Y. Wang, *J. Power Sources*, 243 (2013) 773.
27. R. Phillips, A. Edwards, B. Rome, D. R. Jones and C. W. Dunnill, *Int. J. Hydrogen Energy*, 42 (2017) 23986.
28. C. Rozain and P. Millet, *Electrochim. Acta*, 131 (2014) 160.